Hindawi Publishing Corporation
Mathematical Problems in Engineering
Volume 2016, Article ID 4967937, 10 pages
http://dx.doi.org/10.1155/2016/4967937

Research Article

Compact Wide Frequency Range Fractional-Order Models of Human Body Impedance against Contact Currents

Todd J. Freeborn,[1] Ahmed S. Elwakil,[2,3] and Brent Maundy[4]

[1]*Department of Electrical and Computer Engineering, University of Alabama, P.O. Box 870286, Tuscaloosa, AL 35487, USA*
[2]*Department of Electrical and Computer Engineering, University of Sharjah, P.O. Box 27272, Sharjah, UAE*
[3]*Nanoelectronics Integrated Systems Center (NISC), Nile University, Cairo, Egypt*
[4]*Department of Electrical and Computer Engineering, University of Calgary, 2500 University Drive NW, Calgary, Canada T2N 1N4*

Correspondence should be addressed to Todd J. Freeborn; todd.freeborn@gmail.com

Received 16 December 2015; Accepted 2 February 2016

Academic Editor: Juan J. Trujillo

Three circuit models using constant phase elements are investigated to represent the human body impedance against contact currents from 40 Hz to 110 MHz. The parameters required to represent the impedance are determined using a nonlinear least squares fitting (NLSF) applied to the averaged human body impedance dataset. The three fractional-order models with 4, 6, and 7 parameters are compared to an already existing integer-order, 11-parameter model. Simulations of the fractional-order models impedance are presented and discussed along with their limitations.

1. Introduction

Electrical impedance measurements of biological tissues, also referred to as bioimpedance, quantify the resistance of a material to an injected electrical stimulus. These measurements quantify the passive electrical properties of biological materials to give information about electrochemical processes in tissues and can be used to monitor physiological changes [1]. This is a very active field of research with the potential to develop noninvasive monitoring methods for a wide array of applications that include hydration monitoring during hemodialysis [2], detecting muscle injury [3], and detecting cardiovascular and muscle activity in amputees [4] and as a fluid management system monitoring heart failure [5] with a continued push to determine further health-care applications [6, 7].

Recently concepts from fractional calculus, the branch of mathematics concerning noninteger differentiation and integration, have been imported into this field [8–11] to model the impedance of biological tissues. Fractional-order models have been applied in monitoring necrosis of human tumour xenografts during and/or after hyperthermia treatment [12], investigating age-related changes of dentine to create nondestructive test methods [13], assessing quality of red blood cell suspensions under storage [14], modeling lung impedance [15], impedance of beef and veal meat [16], and numerous others [11].

Concepts from fractional calculus are typically introduced into bioimpedance using circuit elements with a fractional-order impedance. These elements are used to build equivalent networks that represent the measured impedance of the biological tissue or process over a fixed frequency range. Fractional-order elements can be described generally as fractance device with electrical impedance proportional to s^{α} [17], noting that $s^{\alpha} = (j\omega)^{\alpha} = \omega^{\alpha}[\cos(\alpha\pi/2) + j\sin(\alpha\pi/2)]$. The traditional circuit elements (capacitors, resistors, and inductors) are special cases of the general device when the order α is -1, 0, and 1, respectively. Another special case that has been widely used in biology is the Constant Phase Element (CPE) with impedance $Z_{\mathrm{CPE}} = 1/C_{\alpha}s^{\alpha}$, with order α and pseudo-capacitance C_{α}, and with units Farad $\mathrm{sec}^{(\alpha-1)}$. These units were originally proposed in [18] but have rarely been used in literature and are most commonly reported in Farads. The parameter α has been referred to as the dispersion coefficient [11], being attributed to a distribution of relaxation

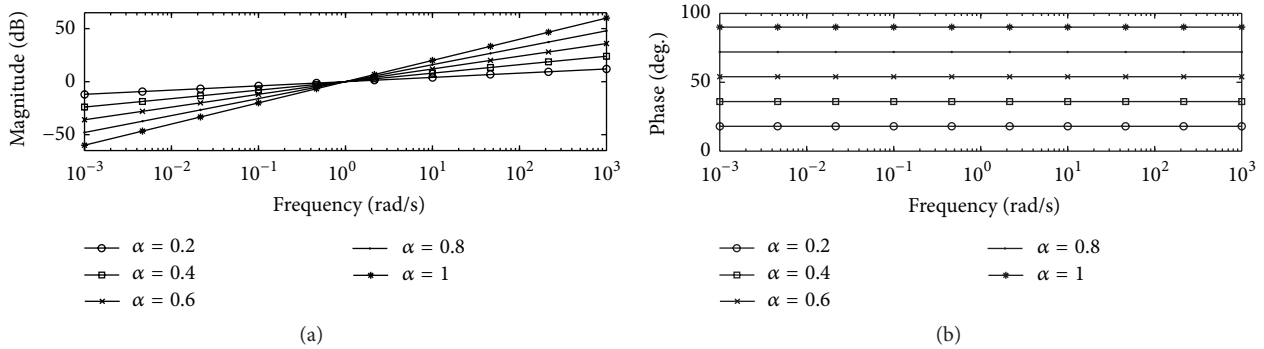

Figure 1: Magnitude and phase response of s^{α} for $\alpha = 0.2, 0.4, 0.6, 0.8$, and 1.0.

times in tissues and a measure of physical processes like the Warburg diffusion [1]. It is important to note that using a CPE implies a fractional derivative of order $0 < \alpha < 1$, with the current-voltage relationship for this component defined as

$$i(t) = C\frac{d^{\alpha}v(t)}{dt^{\alpha}}, \tag{1}$$

where $i(t)$ and $v(t)$ are the time-dependent current and voltage, respectively. When calculating (1) using sinusoidal voltages the fractional derivative must be defined on the whole real line to yield a sinusoidal function. Therefore, the Grunwald-Letnikov, Liouville, and Caputo on $\mathbb{R}$ definitions of fractional derivatives must be used [19]. This is important for impedance applications that are collected in experimental setups that apply a sinusoidal excitation signal and measure the corresponding sinusoidal output. For these cases, the correct definition must be used or else the fractional-order impedance model and experimental results will contradict each other.

A CPE has a constant phase angle, ϕ_{CPE}, independent of frequency given as $\phi_{\text{CPE}} = -\alpha\pi/2$; it is from this property that its name is derived. While $\alpha \in \mathfrak{R}$ is mathematically possible, the values from experimentally collected data of biological tissues are typically in the range $0 < \alpha < 1$. CPEs have also been referred to as fractional-order capacitors in reference to their order which falls between the values of a resistor ($\alpha = 0$) and capacitor ($\alpha = 1$). For reference the magnitude and phase of s^{α} for $\alpha = 0.2$ to 1 in steps of 0.2 are given in Figures 1(a) and 1(b), respectively. The constant phases of 18°, 36°, 54°, 36°, 72°, and 90°, from which CPEs derive their name, are seen in Figure 1(b) for $\alpha = 0.2$ to 1.

Traditionally, integer-order models have been used to represent the impedance of a human body towards contact currents; that is, currents that can flow through the body when contacting a conductive surface at a different potential providing a path for electrical current. At very low levels, this current is not perceived by the subject but above certain thresholds can be uncomfortable and in extreme cases dangerous to the subjects' health. Therefore, it is important to keep contact currents below certain thresholds to prevent pain, burns, breathing difficulty, and in extreme cases cardiac ventricular fibrillation. For example, IEC publications 61010, 60479, and 60601 suggest that contact currents be reduced below 0.01 mA for medical equipment directly applied to patients (with no intentional current insertion), below 0.5 mA to prevent perception, below 5 mA to prevent involuntary muscle contractions, and below 500 mA to prevent tissue damage through electric burns [20]. Models of human body impedance are necessary for the design, simulation, and compliance testing of electrical apparatus that will be contacted by humans to ensure that contact currents are below these thresholds. The IEC 60990 safety standard equivalent circuit for human body impedance is shown in Figure 2(a). This model, composed of a series resistor and parallel resistor-capacitor (RC) cell, was recently shown not to accurately model the impedance of the human body at high and low frequencies [20]. A higher-order integer model was further proposed in [20] and is given in Figure 2(b) but requires 11 components (a series resistor and 5 RC cells).

In this work, we conduct a secondary analysis on the previously collected human body impedance data by De Santis et al. in [20] to explore three compact fractional-order circuit models to represent the impedance of the human body for safety requirements against contact currents. These proposed models employ one or more CPEs, are more compact than integer-order circuit models, and provide good fit for the human body impedance across the frequency range 40 Hz to 110 MHz. The parameters for each model are obtained by applying the method of nonlinear least squares fitting (NLSF) to the averaged human body impedance dataset collected in a previous study [20].

2. Methods

2.1. Human Body Impedance. De Santis et al. previously presented an equivalent circuit in [20] to represent the impedance of the human body to contact currents for safety requirements. This equivalent circuit, given in Figure 2(b), was selected to represent the average impedance collected from a total of 55 living subjects (30 adult males and 25 adult females). The magnitude of this impedance is given in Figure 3 as a solid line, representing the average value computed from each of the 55 individuals over the frequency band from 40 Hz to 110 MHz. This data was collected using a fixed setup configuration with each participant barefoot with wet skin grasping the test apparatus. This setup was

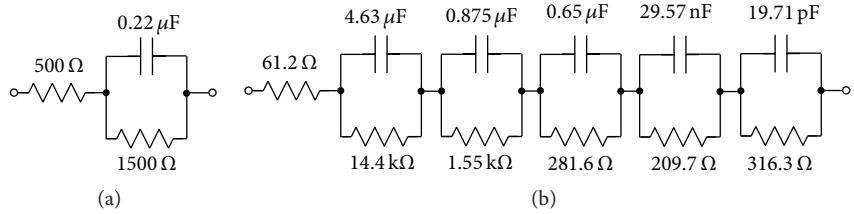

Figure 2: Human impedance model from (a) IEC 60990 safety standard and (b) equivalent network from [20] valid up to 110 MHz.

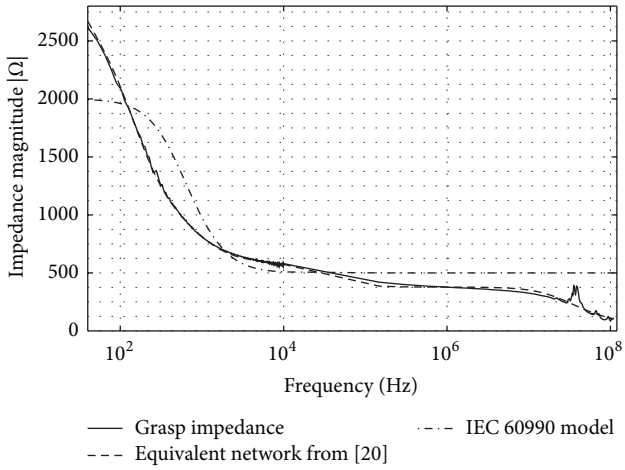

Figure 3: Impedance magnitude of IEC 60990 equivalent network (hatched) and proposed equivalent network from [20] (dashed) compared to human body impedance (solid).

determined in [20] to be the worst case configuration that would yield the lowest impedance, representing the most dangerous situation for a human subject to a contact current. Note that the human impedance is dependent on the type of subject (male, female, and child), electrode characteristics, current path, skin condition, protective clothes, and surrounding environment [20]. For these measurements, each participant was grasping a cylindrical copper electrode with one hand while standing on a large aluminum sheet acting as the second electrode. In this configuration, impedance data was collected from two pieces of measurement equipment, an impedance analyzer (Agilent 4294A) for data from 40 Hz to 1 MHz and a vector network analyzer (HP 8753D) for data from 1 MHz to 110 MHz. The full set of details on the test setups to collect these impedance measurements can be obtained in [20], which includes the employed electrodes and dimensions, experimental setups for both impedance and network analyzers, and descriptions of techniques to reduce lead impedances, contact resistances, and stray capacitances.

The equivalent circuit in Figure 2(b) from [20] requires five capacitors and six resistors to represent this averaged impedance data. The impedance of this network, given in Figure 3 as a dashed line, much more accurately represents the averaged impedance than the IEC model (given as a hatched line). Of significant concern using the IEC model is the difference between the averaged human body impedance and IEC model at frequencies above 100 kHz. Above this frequency the IEC model underestimates the human body impedance, which could lead to contact currents above the safety thresholds when designing safety controls in electrical equipment. It is for this reason that it is important to consider electrical networks that will more accurately represent the human body impedance to a variety of situations.

Fractional-order circuit models have been previously used to represent the impedance of biological tissues in which distributed relaxation times are common making them appropriate for this safety application. Fractional derivatives, upon which these models are based, allow capture of phenomena across multiple time scales overcoming the need to define tissue properties at the cellular level and instead assume they are captured in the fractal structure of the tissue [8, 9]. Recent research has shown the relationship between fractals and fractional calculus, based on physical and geometric considerations [21]. It is noted in [9] that patterns observed in muscle fibers, tendon, and nerve fibers support that the dynamics of these multiscale structures are expressed by fractional-order models. Using these models here could reduce the number or circuit components and parameters required to accurately represent the human body impedance to contact currents. While these fractional-models fail to describe the underlying physiological mechanisms at the unit or cellular level that contribute to the impedance behavior of a tissue, this is not an important factor for this application. The models for these contact-current applications are for simulation or experimental testing and do not need explanation of the physiological processes that determine the impedance, only that the model provides an accurate fit to the data. Therefore, fractional-order models are an attractive compact alternative to represent human body impedance for this application.

2.2. Proposed Circuit Models. Three fractional-order circuit models, given in Figure 4, are investigated to determine their suitability in representing the averaged human body impedance data given in Figure 3. Model one given in Figure 4(a), also known as the Cole-impedance model, has an impedance given by

$$Z_1(s) = R_0 + \frac{R_1}{1 + s^{\alpha_1} C_1 R_1}. \tag{2}$$

This model is composed of two resistors ($R_{0,1}$) and a CPE (C_1, α_1) and has been widely used to represent the impedance of biological tissues in biomedicine for health applications and biology for plant physiology [11]. It has been employed

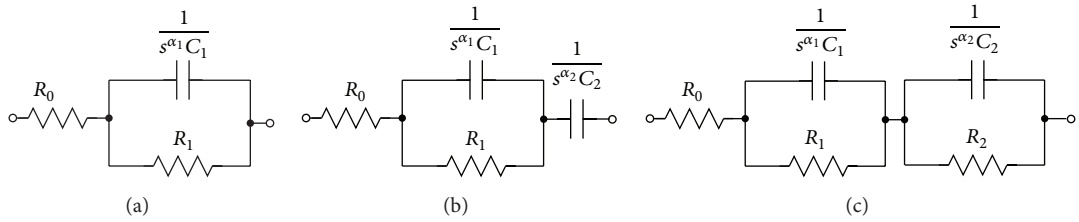

Figure 4: Proposed fractional circuit models to represent the averaged human body impedance data.

in numerous areas because it is simple and compact and has effectively represented impedance of biological tissues over frequency ranges from 30 Hz to 32 MHz in the literature. Model two given in Figure 4(b) is composed of two resistors ($R_{0,1}$) and two CPEs ($C_{1,2}, \alpha_{1,2}$) with impedance given by

$$Z_2(s) = R_0 + \frac{R_1}{1 + s^{\alpha_1} C_1 R_1} + \frac{1}{s^{\alpha_2} C_2}. \tag{3}$$

This model is very similar to that used in [22] to represent the impedance data of a wood sample used to estimate the internal moisture gradients. Model three given in Figure 4(c) is composed of three resistors ($R_{0,1,2}$) and two CPEs ($C_{1,2}, \alpha_{1,2}$) with impedance given by

$$Z_3(s) = R_0 + \frac{R_1}{1 + s^{\alpha_1} C_1 R_1} + \frac{R_2}{1 + s^{\alpha_2} C_2 R_2}. \tag{4}$$

This model has also been referred to as the double dispersion Cole-impedance model in reference to the additional parallel R-CPE cell in series with the single-dispersion Cole-impedance model. This model has been previously used to monitor necrosis of human xenografts [12], characterize intestinal sheep tissue [23], and investigate human dentine [13]. All three models presented here have fewer parameters than the eleven-parameter model of [20], given in Figure 2(b). While there are many other circuit topologies using R-CPE combinations that could be explored, the models in this work were selected to provide a range of increasing complex fractional-models that have fewer parameters than the model in Figure 2(b). It should be noted that while fractional calculus and by extension fractional-order circuit models do show a relationship with fractal structures and patterns [21], the models here were not selected based on any observations of fractal structures of the biological tissues of a human body, although this would provide an insightful and interesting avenue to further explore and justify fractional-order models for representing the human body and further improve the models used.

2.3. Nonlinear Least Squares Fitting. To analyze the suitability of each fractional-order model to represent the human body impedance data requires determining the circuit parameters for each of the models that provide the best fit to the data. To determine these parameters a Nonlinear Least Square Fitting (NLSF) optimization routine is employed. This NLSF was previously used in [24] to extract the impedance parameters of both single and double dispersion Cole-impedance model parameters from magnitude-response datasets, not requiring direct impedance measurements. This process is adapted here to determine the parameters of the models presented in Table 1 using the impedance magnitude data given in Figure 2. The NLSF attempts to numerically solve the problem

$$\begin{aligned} \min_x \quad & f_0(x) = \sum_{j=1}^{n} \left(\left| Z\left(x, \omega_j\right) \right| - y_j \right)^2 \\ \text{s.t.} \quad & x > 0, \end{aligned} \tag{5}$$

where x is the set of impedance parameters to minimize $f_o(x)$, $|Z(x, \omega_j)|$ is the impedance magnitude for a given circuit model at frequency ω_j, y_j is the human body impedance at frequency ω_j, and n is the total number of data points in the collected response. A constraint is added to the problem to limit the possible solutions to real values; because negative resistance and capacitance values are not physically possible. Also, a negative value dispersion coefficient (α) indicates inductive characteristics which is not considered here.

To begin, the NLSF method requires an initial condition, x_0, from which to start iteratively solving towards a solution x^*. This NLSF method was implemented using the MATLAB *lsqcurvefit* function configured to quit searching for a solution when any of the following conditions are satisfied during each iteration:

(i) The number of function evaluations exceeds 1000.

(ii) The change in the value of x is less than 1×10^{-9}.

(iii) The change in the function value is less than 1×10^{-9}.

After quitting due to satisfying any of the ending criteria, the solver returns a possible solution. However, there may be many local minima that satisfy the ending criteria without being the true global solution. Therefore, the solver has the potential to return solutions that are not the optimum parameters. A method proposed in [24] to improve the likelihood of returning the global solution executed the solver multiple times using a new randomly generated initial condition, x_0, each time. The intent is to generate an initial starting condition very close to the global solution so that when the ending criteria are met the solver has found the global solution and avoided returning local minima. A simplified overview of this process is given in Figure 5. Each of the five grey circles, labelled (1)–(5), indicates an initial condition that the solver begins iteratively solving from to find the global solution (represented by the large black circle). Assuming the

Table 1: Average and standard deviation of circuit models parameters and LSE from NLSF parameters for models one, two, and three to represent human impedance data.

Model		LSE	R_0 (Ω)	R_1 (Ω)	R_2 (Ω)	C_1 (F sec$^{\alpha_1-1}$)	C_2 (F sec$^{\alpha_2-1}$)	α_1	α_2
One	Avg.	8.83×10^6	186.3	517.5 k	—	64.13 μ	—	0.347	—
	Std. Dev.	33.29	0.183 m	271.3 k	—	0.307 n	—	0.442 μ	—
Two	Avg.	2.33×10^6	9.44	441.4	—	11.8 n	19.0 μ	0.663	0.539
	Std. Dev.	0.881 m	14.2	20.6	—	7.9 n	2.1 μ	0.04	0.02
Three	Avg.	1.19×10^6	1.22	3.72 k	523.6	4.36 μ	20.0 n	0.722	0.628
	Std. Dev.	63.4 k	3.15	2.42 k	14.5	2.2 μ	15.3 n	0.04	0.02

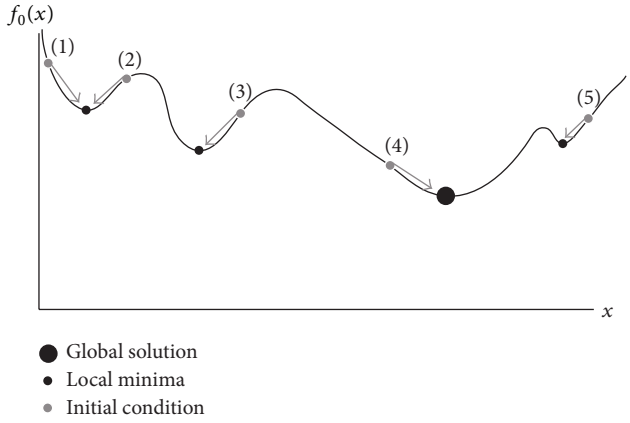

Figure 5: Simplified example using multiple initial conditions to increase likelihood of returning global solution using optimization.

solver is applied to initial conditions (1) to (5), in that order, the solver will return four different solutions. Three of which will be local minima represented by the smaller black circles. These local minima are not the global solution even though they will satisfy the stopping criteria of the solver. The arrow on each initial condition indicates the solution direction that the solver will take towards one of the possible solutions. Only solving from initial condition (4), in this example, will return the global solution. Therefore, solving from each initial condition and selecting the case which returns the lowest function value ($f_0(x)$) yield the global solution, though this process does not guarantee the return of the global solution. If only four initial conditions were used, and (4) was omitted (see Figure 5), the retuned solution would not be the global solution. This can be overcome by increasing the number of executions using new initial conditions but comes at the cost of increasing the total time required to solve for the function minimum. In [24] the solver was run 20 and 60 times to extract the circuit model parameters from models with 4 and 7 parameters, respectively.

In this work, 20, 100, and 200 executions of the solver with randomly generated initial conditions were applied to determine the impedance parameters for models one, two, and three, respectively. Each set of initial conditions was randomly generated within the ranges 1 mΩ $< R_{0,1,2} <$ 1 GΩ, 1 fF $< C_{1,2} <$ 1 mF, and $0 < \alpha_{1,2} < 1$. The MATLAB code for the implementation of this NLSF process to solve for the parameters for model one is given in Algorithm 1. Note that in this algorithm the human body impedance data is stored in the variable Z and the frequencies (in rad/s) for each datapoint in Z are given in the variable w.

3. Results

The averaged component parameters (and their standard deviations) returned by the NLSF process for each model are given in Table 1. The simulated impedances from 40 Hz to 110 MHz using these values are given in Figure 6(a) with the errors of each compared to the grasping impedance data given in Figure 6(b). In both figures the red, magenta, and blue lines correspond to models one, two, and three, respectively, while the solid black line in Figure 6(a) is the experimental impedance data used for the fitting and in Figure 6(b) is the error between the experimental impedance data and the equivalent network parameters from [20]. The trend of improving fit with increasing parameters is reflected in the maximum error between the simulated impedance and the experimental results. Models one, two, and three have maximum errors of 133.7%, 65.8%, and 55.5%, respectively. Though all models have a higher maximum error than the proposed network in [20] which is 30.7%, model three in the low-frequency band (40 Hz to 10 kHz) has a lower maximum error of 2.8% compared to 4.2% in the integer model. Even with model one having higher error over mid-frequencies (10 kHz to 10 MHz) it has similar error at high frequencies (10 MHz to 110 MHz) compared to the integer model in [20].

To verify that the NLSF process (solving using multiple randomly generated initial conditions) converged to a similar solution for each circuit parameter of each model, it was applied 20 times for each model and the least squares error (LSE) of each was monitored. The evolution of the LSE is given in Figures 7(a), 7(c), and 7(e) for models one, two, and three, respectively. The LSEs were calculated using

$$\text{LSE} = \sum_{i=1}^{k} \left(\left| Z\left(x, \omega_j\right) \right| - y_j \right)^2, \tag{6}$$

where Z is the impedance of the fractional-order models using (2), (3), or (4), x is the vector of circuit parameters for that model, and y is the averaged human body impedance dataset. For this evolution, the minimum LSE is only updated if the LSE from the execution with the current initial condition is lower than the previous value. Bands where the LSE is flat indicate that the LSE returned from those iterations were not lower than the previous iteration. In each

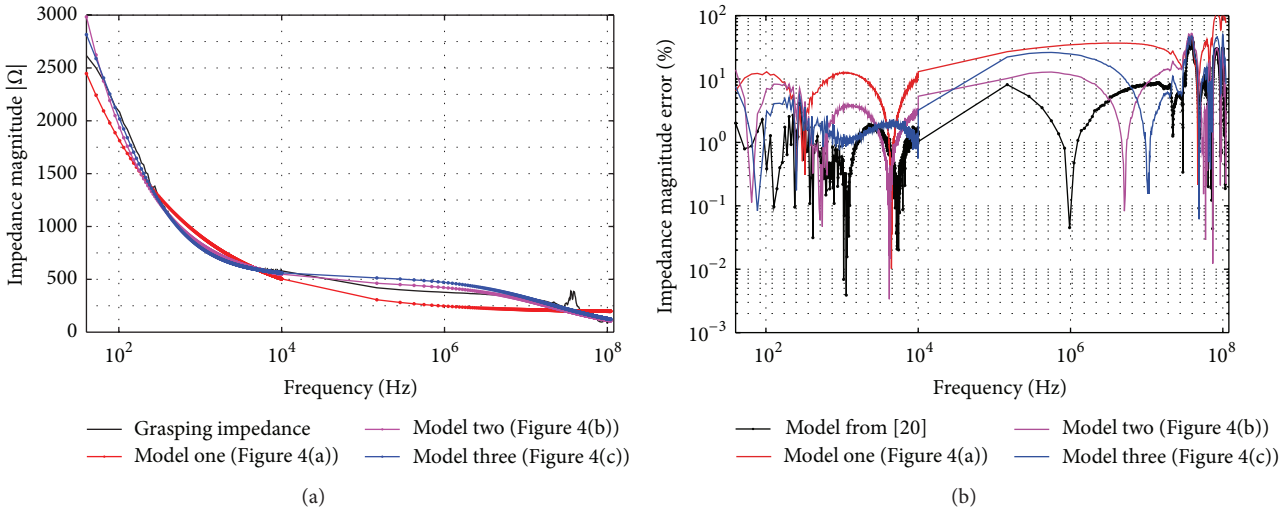

FIGURE 6: (a) Simulated impedance magnitudes and (b) errors compared to experimental data for models one (red), two (magenta), and three (blue).

of Figures 7(a), 7(c), and 7(e) all 20 trials converge towards a common LSE as the number of executions using new initial conditions increases, with the number of initial conditions required to converge also increasing with increasing model complexity. Model one required 8 initial conditions for each trial to converge, model two required approximately 60, and model three required approximately 150. The average LSE of the 20 trials for each model is 8.827×10^6, 2.333×10^6, and 1.947×10^6 for models one, two, and three. Note that the differences in LSE for each trial at the final initial condition appear significant due to the presentation of the y-axis data on a log scale which magnifies the appearance of their small differences. The standard deviation of the LSEs from all the trials is 33.29, 8.81×10^4, and 6.34×10^4 for models one, two, and three, respectively. For comparison the network proposed in [20] has a LSE of 1.32×10^6. Therefore, model three and the network of [20] have similar LSEs but the fractional model requires 4 fewer parameters.

For further comparison of the parameter differences from each of the 20 NLSF trials, the values from each trial are given in Figures 7(b), 7(d), and 7(f) for models one, two, and three, respectively. From Figure 7(b), the values for R_0, C_1, and α_1 are stable over all trials, though R_1 has a large variation between trials which is also reflected in its large standard deviation (given in Table 1). These values range from 34.3 kΩ to 967 kΩ with no significant change in the LSE, indicating that while the impedance of this model requires a value of $R_1 > 30$ kΩ the LSE is not significantly impacted by the value if it is above this floor. Similarly the values of each component for models two and three are relatively constant in Figures 7(d) and 7(f), respectively, with the exception of R_0 for both models. The value of R_0 shows a variation from 59.6 mΩ to 52.0 Ω for model two and from 9.9 μΩ to 12.9 Ω for model three, again with very little impact on the LSE for this model. To further investigate the impact of this component on the LSE and determine if it is actually required to represent the human body impedance, the LSE was calculated using (6) when $R_0 = 0$ for both models two and three. The LSEs for models two and three for this case were 3.18×10^6 and 2.11×10^6, respectively, compared to the original LSE values of 2.78×10^6 and 2.09×10^6. There is very little change for model three when $R_0 = 0\,\Omega$ while there is a larger change in the LSE for model two. Therefore R_0 does not appear significant and could be removed from model three without significant reduction in LSE and model fit to the impedance data. The impedance magnitude error between models two and three and the human body data are given in Figure 8. The errors using the values of R_0 from Table 1 are given as solid lines and the errors when $R_0 = 0$ are given as circles. Model two has a larger impedance error when $R_0 = 0$ above 5 MHz, which is likely the source of the larger LSE, while model three has a very similar impedance error over the entire frequency range. Of significant note is the fact that when $R_0 = 0\,\Omega$ model three has lower LSE (2.11×10^6) than model two using R_0 from Table 1 (2.78×10^6) even though both are 6-parameter circuit models.

Comparing the impedance of the IEC 90990 network, given in Figure 3 as a hatched line, to the proposed human body impedance, given in Figure 3 as a solid line, it is clear that the IEC model does not provide an accurate fit of the human body impedance over this frequency range. The IEC model error compared to the experimental data is given in Figure 9 as a dashed line and has a maximum error of 489.8%, an average error of 116.3%, and LSE of 1.34×10^8, two orders of magnitude larger than the LSE of all the fractional-order models. While models two and three have a better fit than model one, it is worth noting that if the intent is to keep a compact and simple model to represent the human body impedance, then using model one over the IEC model significantly increases the accuracy while only increasing the number of circuit parameters by one. Further, it would decrease the maximum error to 133.7% and decrease the average error to 28.3%. For comparison, the error of model one is also given in Figure 9 as a blue line; model one and

```
(1) procedure NLSF-Multiple Initial Conditions
      // Boundaries for initial condition generation [R0, R1, C, α]
(2)   LB1 = [−1, −1, −15, 0];
(3)   UB1 = [9, 9, −3, 1];
      // Boundaries for lsqcurvefit function [R0, R1, C, α]
(4)   LB2 = [0, 0, 0, 0];
(5)   UB2 = [inf, inf, inf, inf];
      // Setting up vector for initial conditions
(6)   x0 = zeros(20, 4);
(7)   [R, C] = size(x0);
      // Setting lsqcurvefit stopping conditions
(8)   options = optimset("lsqcurvefit");
(9)   options.MaxFunEvals = 1000;
(10)  options.TolX = 1e − 9;
(11)  options.TolFun = 1e − 9;
      // Generating array of initial conditions
(12)  for k = 1:1:length(x0) do
(13)    for i = 1:1:C do
(14)      x0(:, i) = LB1(i) + (UB1(i) − LB1(i)).∗rand(R, 1);
(15)    end for
(16)    x0(:, 1) = 10.^x0(:, 1);
(17)    x0(:, 2) = 10.^x0(:, 2);
(18)    x0(:, 3) = 10.^x0(:, 3);
(19)    MinLSE = inf;
(20)    for j = 1:1:R do
(21)      [ModelParameters, LSE] = lsqcurvefit(@ModelOneImpedance, x0(j, :), w, Z, LB2, UB2, options);
(22)      if LSE < MinLSE do
(23)        BestModelParameters = ModelParameters;
(24)        MinLSE = LSE;
(25)      end if
(26)    end for
(27)  end for
(28) end procedure
(29) function ModelOneImpedance(ModelParameters, w)
(30)  s = 1i ∗ w;
(31)  R0 = ModelParameters(1);
(32)  R1 = ModelParameters(2);
(33)  C = ModelParameters(3);
(34)  alpha = ModelParameters(4);
(35)  Z = R0 + R1./(1 + s.^(alpha) ∗ C ∗ R1);
(36)  return abs(Z);
(37) end function
```

Algorithm 1: MATLAB implementation of NLSF using *lsqcurvefit* with multiple initial conditions.

the IEC model have similar errors from 10 kHz to 40 MHz but the fractional-order model significantly improves the fit at low and high frequencies.

4. Limitations

While fractional-order models can represent the human body impedance and have a wide range of applications for modeling biological tissues, they also have limitations in regard to their simulation and realization. Integer-order models can be easily simulated since resistors, capacitors, and inductors are standard components within circuit simulators. However, at this time, CPEs are not supported and require integer-order approximations, typically realized using RC ladder topologies [25, 26] or specialized software such as EIS or Z-View, to be simulated. Using an RC ladder topology to realize the CPEs removes the advantage of fewer parameters and requires greater effort and specialized knowledge to be implemented, though it is possible to easily work with fractional-order models using MATLAB which has an array of tools available for numerical simulations, making comparison of mathematical models and experimental data straightforward. Also, integer models can be quickly realized with widely available off-the-shelf components, which makes their assembly a simple matter of collecting the correct components. Similar to their simulation, the fractional-order models can currently only be built using approximations with passive or active topologies, again, removing the advantages

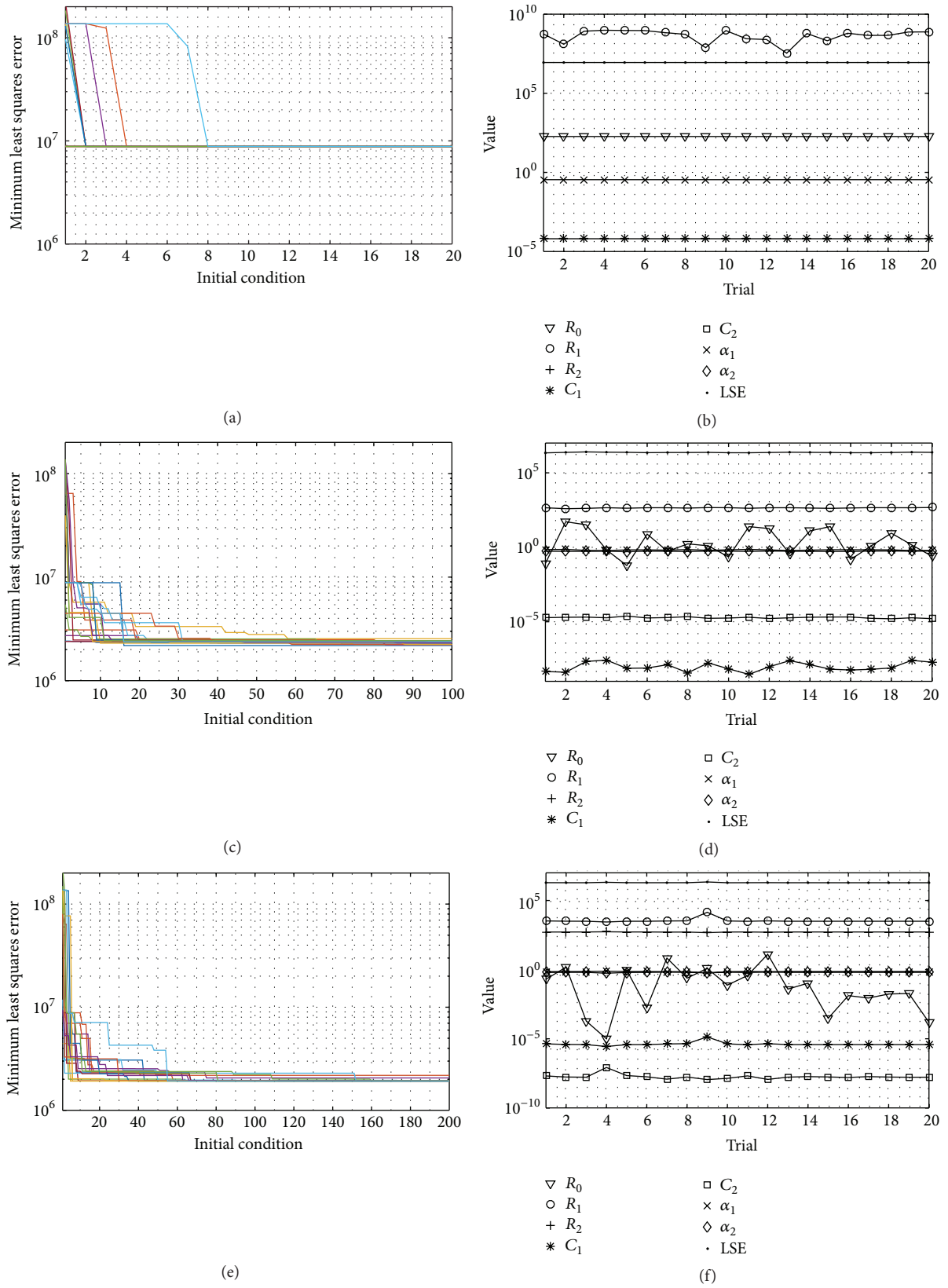

FIGURE 7: (a), (c), (e) Evolution of LSE from the NLSF when multiple initial conditions applied and (b), (d), (f) parameter variation from multiple trials of the NLSF.

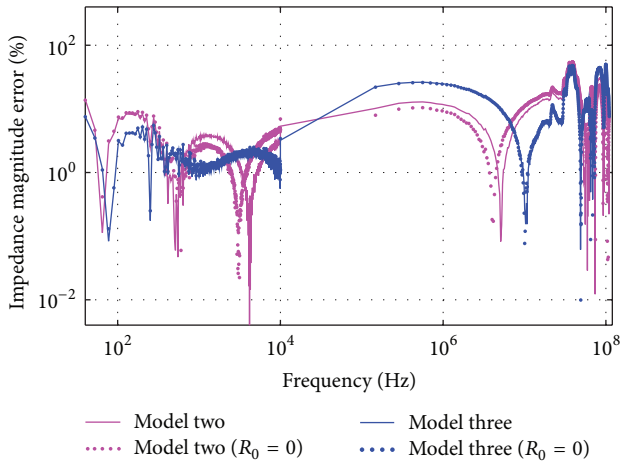

FIGURE 8: Simulated impedance magnitude errors for models two (magenta) and three (blue) compared to experimental data with R_0 from Table 1 (solid lines) and $R_0 = 0\,\Omega$ (circles).

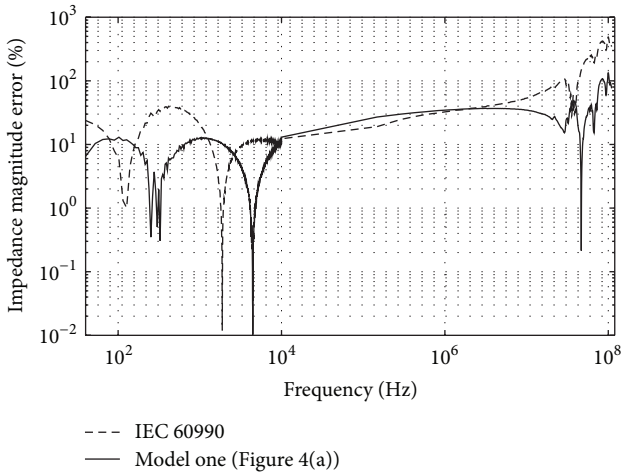

FIGURE 9: Errors of IEC 60990 safety model (dashed) and fractional Model #1 (blue) compared to experimental data.

offered by the fewer parameters and requiring greater effort to design and implement these models. Though there is progress towards realizing fractional-order elements [27–29] with the hope that they will be commercially available to take advantage of their unique characteristics without requiring specialized knowledge of their realization to build and implement fractional-order circuits. These areas are exciting opportunities for future research to be conducted to advance the adoption of fractional-order models into circuits and systems, thereby furthering our knowledge and insight into these fields, all the while exploring the new applications that they open up.

5. Conclusion

This work analyzed the use of fractional-order circuit models to represent the averaged human body impedance to contact currents over the frequency 40 Hz to 110 MHz. A simple fractional-order model with 4 terms significantly increased the accuracy of representing this impedance over the IEC human body model, while a 7-term model was the most accurate at representing the impedance with similar errors to an 11-term integer-order model. This highlights the strength of fractional-order models in providing compact, accurate models of biological data providing wide frequency range coverage.

Conflict of Interests

The authors declare that there are no conflict of interests regarding the publication of this paper.

Acknowledgment

The authors would like to thank Valerio De Santis and Mauro Feliziani from the University of L'Aquila, Italy, for sharing their experimental data regarding human body impedance against contact currents for the analysis in this work.

References

[1] S. Grimnes and Ø. G. Martinsen, *Bioimpedance and Bioelectricity Basics*, Academic Press, London, UK, 2nd edition, 2008.

[2] F. Zhu, M. K. Kuhlmann, P. Kotanko, E. Seibert, E. F. Leonard, and N. W. Levin, "A method for the estimation of hydration state during hemodialysis using a calf bioimpedance technique," *Physiological Measurement*, vol. 29, no. 6, pp. S503–S516, 2008.

[3] G. Hornero, D. Díaz, and O. Casas, "Bioimpedance system for monitoring muscle and cardiovascular activity in the stump of lower-limb amputees," *Physiological Measurement*, vol. 34, no. 2, pp. 189–201, 2013.

[4] L. Nescolarde, J. Yanguas, H. Lukaski, X. Alomar, J. Rosell-Ferrer, and G. Rodas, "Localized bioimpedance to assess muscle injury," *Physiological Measurement*, vol. 34, no. 2, pp. 237–245, 2013.

[5] S. Weyer, M. D. Zink, T. Wartzek et al., "Bioelectrical impedance spectroscopy as a fluid management system in heart failure," *Physiological Measurement*, vol. 35, no. 6, pp. 917–930, 2014.

[6] S. R. Atefi, F. Seoane, T. Thorlin, and K. Lindecrantz, "Stroke damage detection using classification trees on electrical bioimpedance cerebral spectroscopy measurements," *Sensors*, vol. 13, no. 8, pp. 10074–10086, 2013.

[7] S. L. Swisher, M. C. Lin, A. Liao et al., "Impedance sensing device enables early detection of pressure ulcers *in vivo*," *Nature Communications*, vol. 6, article 6575, 2015.

[8] R. L. Magin, *Fractional Calculus in Bioengineering*, Begell House, West Redding, Conn, USA, 2006.

[9] R. L. Magin, "Fractional calculus models of complex dynamics in biological tissues," *Computers & Mathematics with Applications*, vol. 59, no. 5, pp. 1586–1593, 2010.

[10] R. Magin, M. D. Ortigueira, I. Podlubny, and J. Trujillo, "On the fractional signals and systems," *Signal Processing*, vol. 91, no. 3, pp. 350–371, 2011.

[11] T. J. Freeborn, "A survey of fractional-order circuit models for biology and biomedicine," *IEEE Journal on Emerging and Selected Topics in Circuits and Systems*, vol. 3, no. 3, pp. 416–424, 2013.

[12] D. A. McRae, M. A. Esrick, and S. C. Mueller, "Changes in the noninvasive, in vivo electrical impedance of three xenografts during the necrotic cell-response sequence," *International Journal of Radiation Oncology Biology Physics*, vol. 43, no. 4, pp. 849–857, 1999.

[13] A. H. Eldarrat, D. J. Wood, G. M. Kale, and A. S. High, "Age-related changes in ac-impedance spectroscopy studies of normal human dentine," *Journal of Materials Science: Materials in Medicine*, vol. 18, no. 6, pp. 1203–1210, 2007.

[14] Y. Ulgen and M. Sezdi, "Hematocrit dependence of the Cole-Cole parameters of human blood," in *Proceedings of the 2nd International Conference Biomedical Engineering Days*, pp. 71–74, Istanbul, Turkey, May 1998.

[15] C. M. Ionescu, J. A. T. Machado, and R. De Keyser, "Modeling of the lung impedance using a fractional-order ladder network with constant phase elements," *IEEE Transactions on Biomedical Circuits and Systems*, vol. 5, no. 1, pp. 83–89, 2011.

[16] M. Guermazi, O. Kanoun, and N. Derbel, "Investigation of long time beef and veal meat behavior by bioimpedance spectroscopy for meat monitoring," *IEEE Sensors Journal*, vol. 14, no. 10, pp. 3624–3630, 2014.

[17] M. Nakagawa M and K. Sorimachi, "Basic characteristics of a fractance device," *IEICE Transactions on Fundamentals of Electronics Communications and Computer Sciences*, vol. 75, pp. 1814–1819, 1992.

[18] S. Westerlund and L. Ekstam, "Capacitor theory," *IEEE Transactions on Dielectrics and Electrical Insulation*, vol. 1, no. 5, pp. 826–839, 1994.

[19] M. D. Ortigueira, J. Tenreiro Machado, and J. J. Trujillo, "Fractional derivatives and periodic functions," *International Journal of Dynamics and Control*, pp. 1–7, 2015.

[20] V. De Santis, P. A. Beeckman, D. A. Lampasi, and M. Feliziani, "Assessment of human body impedance for safety requirements against contact currents for frequencies up to 110 MHz," *IEEE Transactions on Biomedical Engineering*, vol. 58, no. 2, pp. 390–396, 2011.

[21] S. Butera and M. Di Paola, "A physically based connection between fractional calculus and fractal geometry," *Annals of Physics*, vol. 350, pp. 146–158, 2014.

[22] M. Titta and H. Oikkonen, "Electrical impedance spectroscopy device for measurement of moisture gradients in wood," *Review of Scientific Instruments*, vol. 73, no. 2, pp. 159–166, 2015.

[23] B. Rigaud, L. Hamzaoui, M. R. Frikha, N. Chauveau, and J.-P. Morucci, "In vitro tissue characterization and modelling using electrical impedance measurements in the 100 Hz-10 MHz frequency range," *Physiological Measurement*, vol. 16, pp. A15–A28, 1995.

[24] T. J. Freeborn, B. Maundy, and A. S. Elwakil, "Extracting the parameters of the double-dispersion Cole bioimpedance model from magnitude response measurements," *Medical and Biological Engineering and Computing*, vol. 52, no. 9, pp. 749–758, 2014.

[25] D. Stancic, J. Q. Fang, and I. Cosic, "Distributed biological tissue impedance model for SPICE simulation," in *Proceedings of the International Symposium on Bioelectronics and Bioinformatics*, pp. 201–205, Melbourne, Australia, December 2009.

[26] J. Valsa and J. Vlach, "RC models of a constant phase element," *International Journal of Circuit Theory and Applications*, vol. 41, no. 1, pp. 59–67, 2013.

[27] T. C. Haba, G. L. Loum, and G. Ablart, "An analytical expression for the input impedance of a fractal tree obtained by a microelectronical process and experimental measurements of its non-integral dimension," *Chaos, Solitons & Fractals*, vol. 33, no. 2, pp. 364–373, 2007.

[28] M. Sivarama Krishna, S. Das, K. Biswas, and B. Goswami, "Fabrication of a fractional order capacitor with desired specifications: a study on process identification and characterization," *IEEE Transactions on Electron Devices*, vol. 58, no. 11, pp. 4067–4073, 2011.

[29] A. M. Elshurafa, M. N. Almadhoun, K. N. Salama, and H. N. Alshareef, "Microscale electrostatic fractional capacitors using reduced graphene oxide percolated polymer composites," *Applied Physics Letters*, vol. 102, no. 23, Article ID 232901, 2013.